A CHARACTERISTICS-BASED IMPLICIT FINITE-DIFFERENCE SCHEME FOR THE ANALYSIS OF INSTABILITY IN WATER COOLED REACTORS

GOUTAM DUTTA and JAGDEEP B. DOSHI*
Department of Mechanical Engineering
Indian Institute of Technology Bombay Powai, Mumbai: 400076, India
*Corresponding author. E-mail : doshi@me.iitb.ac.in

Received March 5, 2008
Accepted for Publication June 30, 2008

The objective of the paper is to analyze the thermally induced density wave oscillations in water cooled boiling water reactors. A transient thermal hydraulic model is developed with a characteristics-based implicit finite-difference scheme to solve the nonlinear mass, momentum and energy conservation equations in a time-domain. A two-phase flow was simulated with a one-dimensional homogeneous equilibrium model. The model treats the boundary conditions naturally and takes into account the compressibility effect of the two-phase flow. The axial variation of the heat flux profile can also be handled with the model. Unlike the method of characteristics analysis, the present numerical model is computationally inexpensive in terms of time and works in a Eulerian coordinate system without the loss of accuracy. The model was validated against available benchmarks.

The model was extended for the purpose of studying the flow-induced density wave oscillations in forced circulation and natural circulation boiling water reactors. Various parametric studies were undertaken to evaluate the model's performance under different operating conditions. Marginal stability boundaries were drawn for type-I and type-II instabilities in a dimensionless parameter space. The significance of adiabatic riser sections in different boiling reactors was analyzed in detail. The effect of the axial heat flux profile was also investigated for different boiling reactors.

KEYWORDS : Two-Phase Flow, Instability, Boiling Water Reactor, Density Wave Oscillations

1. INTRODUCTION

Two-phase flow systems are prone to dynamic and static instabilities of many kinds. In the last few decades, a considerable amount of work on the two-phase flow instability has been carried out all over the world. Several numerical, experimental and analytical studies were conducted to understand two-phase flow instabilities and to derive the stability criteria. Theoretical modelling of density wave oscillation (DWO) stability analysis can be divided into two major groups: frequency-domain analysis and time-domain analysis. Frequency-domain analysis is based on the linearization of nonlinear equations by perturbing the governing equations around a steady-state point. Once this linear model has been converted from a time domain to a frequency domain, exact analytical solutions can be obtained. As a result, marginal stability boundaries (MSBs) in a parameter space can be determined and the space is divided into stable and unstable regions. The nonlinear time domain approach relies on a digital numerical simulation of nonlinear partial differential equations (PDEs) by means of finite-difference techniques. This approach is more accurate and suitable for limit cycle oscillations. The principal disadvantages of models based on this approach are tedious computations, numerical instabilities of algebraic equations and time-step constraints. Recent advances in high-speed computers and sophisticated finite-difference models have resulted in significant economic advantages and design confidence. Accuracy is no longer an expense or inconvenience. Consequently, the study of the nonlinear behavior of DWOs has attracted considerable interest.

Hancox and Banerjee presented a benchmark solution procedure that is based on a method of characteristics analysis (MECA) and applicable to the Lagrangian coordinate system [1, 2]. They presented various numerical methodologies for the development of loss of coolant accident analysis, including two different finite-difference techniques: an explicit finite-difference

technique and an implicit scheme called a technique of "characteristic finite difference". Next, Ferch presented an equal-velocity unequal-temperature model together with a characteristics algorithm [3]. Although accurate results were obtained with these wave tracing procedures, the procedures were computationally slow and difficult to apply to geometrically complex problems.

There are several other techniques, such as the semi-implicit method of field equations, that try to solve the two-phase flow dynamics problems by using the drift flux approximation introduced by Liles and Reed [4]. However, such methods involve tedious mathematical formulations associated with discontinuous property derivatives at boiling boundaries. A simple algorithm, called SPORTS, was developed by Chatoorgoon [5] for two-phase flow boiling systems. Prasad et al. [6] used a thermal hydraulics model proposed by the SPORTS code, as well as point kinetics equations for neutron dynamics, to conduct a comprehensive investigation of nuclear-coupled DWOs in a boiling water reactor (BWR/6). Narayanan et al. [7] analyzed DWOs in a vertical heated channel by using a simplified model with assumptions of constant properties at a given system pressure. However, natural treatment of different boundary conditions with these models is not possible; rather, a "shooting method" must be applied to fix the pressure drop boundary conditions that are applicable to parallel boiling channels of the reactor core. In another approach, Lin and Pan [8] investigated the nonlinear dynamics of a two-phase natural circulation (NC) boiling channel by using the Galerkin nodal approximation method. The method transforms the PDEs into a set of ordinary differential equations.

A linear stability analysis in the frequency domain was performed by Wang et al. [9] to establish the stability map of an NC loop for different parametric conditions. Their study confirms the presence of type-I instability when the heated section has a low exit quality. Bragt and Hagen developed a theoretical model based on a frequency domain approach for coupled neutronic-thermohydraulic power oscillations in a Dutch Dodewaard NC BWR [10]. Their neutron kinetics model consists of point-kinetics equations with one effective delayed neutron group. In a companion paper, the same authors subsequently performed a parametric study to identify the main parameters that determine the model's stability [11]. They reported that the type-I instability emerges in the reactor with the introduction of an adiabatic riser section. In all these studies, the type-II stability boundary shifts to significantly higher power levels when the riser length increases, whereas a longer riser length increases the type-I instability region. The above phenomenon is in contrast to the trend predicted by Rizwan-uddin and Dorning [12]. They found that the presence of a riser has a destabilizing effect on the system. A frequency domain analysis was carried out by Rizwan-uddin [13] to study how different heat flux profiles affect the two-phase flow heated channels that operate in different regions of the parameter space. Reports on the importance of boiling boundary dynamics in stability analysis conlude that the bottom-peaked power profile moves down the boiling boundary location, causing the channel to become less stable.

In the present paper, we adopted the implicit characteristics-based finite-difference scheme proposed by Hancox and Banerjee to analyze the DWOs in BWRs. After developing the model, we compared the results with the MECA results [1]. Compared to MECA, our model is more flexible, computationally faster and reasonably accurate. Next we used the model to simulate the DWOs in forced circulation (FC) flow-boiling systems, and we drew a stability map to compare the results with an experimental benchmark. The model was then extended, firstly, to simulate the in-phase mode of DWOs in both NC and FC BWRs for a single boiling channel lying in the reactor core and, secondly, to quantify the effects of riser sections for various BWRs. The feedback mechanisms of type-I and type-II instabilities related to NC and FC BWRs are different, and this difference may have led to the conflicting ideas in the literature about riser sections. Hence, we made a detailed investigation of FC and NC BWRs separately to understand how they behave when the riser is installed. Furthermore, we studied the effect of different heat flux shapes on NC and FC BWRs in the operational domain and examined whether the behavioral pattern changes for different water circulation modes of the cooling systems used in the reactors.

2. ANALYSIS OF INSTABILITY IN A SINGLE BOILING CHANNEL

A theoretical model was developed to analyze the hydrodynamics of a system of parallel boiling channels connected between two large plena, one at the inlet and the other at the exit. If the pressure drop between the plena remains constant even if the flow rates at the inlet to some channels oscillate, each oscillating channel can be analyzed separately by using the (given) constant pressure drop boundary condition. A similar effect can be obtained by connecting a heated boiling channel in parallel with a single-phase adiabatic bypass channel of large diameter. If the bypass flow rate is much larger than that at the inlet to the boiling channel, the pressure drop between the plena remains constant even if the channel inlet flow is subjected to oscillations.

2.1 Mathematical Model Formulation

The thermal hydraulics model is based on a set of field and constitutive equations and boundary conditions. The assumptions made in the analysis are as follows:

1. No consideration is given to the temperature, pressure and velocity variation in the radial (r) and azimuthal (θ) direction.
2. One-dimensional conservation equations in the axial (z) direction are used.
3. At any cross section, the vapor and liquid phases move at equal velocity and equal temperature (EVET) or are homogeneously mixed and exist in a thermodynamic equilibrium.
4. Only bulk boiling is considered and subcooled boiling is neglected.

The basic one-dimensional conservation equations for the homogeneous two-phase fluid flow model are as follows:

$$\frac{\partial}{\partial t}(\rho A)+\frac{\partial}{\partial z}(\rho A u)=0 \tag{1}$$

$$\frac{\partial}{\partial t}(\rho A u)+\frac{\partial}{\partial z}(\rho A u^2)=-A\frac{\partial p}{\partial z}-\tau_w P_w-\rho A g\frac{dH}{dz} \tag{2}$$

$$\frac{\partial}{\partial t}(\rho A e)+\frac{\partial}{\partial z}(\rho A u e_f)=\dot{Q}'' P_H, \tag{3}$$

where

$$e=e_f-\frac{p}{\rho}$$

and

$$e_f=h+\frac{u^2}{2}+gH.$$

These equations can be written in the following form:

$$\frac{\partial}{\partial t}(\rho A e)+\frac{\partial}{\partial z}(\rho A u e_f)=\dot{Q}'' P_H, \tag{4}$$

where

$$\underline{\mathbf{R}}=\begin{bmatrix}\rho A\\ \rho A u\\ \rho A e\end{bmatrix},\underline{\mathbf{S}}=\begin{bmatrix}\rho A u\\ A\left(\rho u^2+p\right)\\ \rho A u\, e_f\end{bmatrix} \tag{5}$$

and

$$\underline{\mathbf{T}}=\begin{bmatrix}0\\ p\dfrac{dA}{dz}-\tau_w P_w-\rho A g\dfrac{dH}{dz}\\ \dot{Q}_w'' P_H\end{bmatrix}.$$

These conservative forms of the governing equations are converted into a primitive form and written as

$$\frac{\partial}{\partial t}[\,\underline{\mathbf{U}}\,]+\underline{\underline{\mathbf{A}}}(\underline{\mathbf{U}})\frac{\partial}{\partial z}[\,\underline{\mathbf{U}}\,]=[\,\underline{\mathbf{D}}(\underline{\mathbf{U}})\,], \tag{6}$$

where $\underline{U}$ is a vector of unknown variables, $\underline{\underline{A}}$ is a square matrix of coefficients that are functions of $\underline{U}$, and $\underline{D}$ is a vector containing allowances for the mass, momentum, and energy transfer across the system boundaries and between phases. The unknown variables are

$$\underline{\mathbf{U}}=\begin{bmatrix}W\\ h\\ p\end{bmatrix}.$$

In our case, namely the EVET model, the $\underline{\underline{A}}$ matrix and $\underline{D}$ vector are as follows:

$$\underline{\underline{\mathbf{A}}}=\begin{bmatrix}\dfrac{2W}{\rho A} & -\left[\dfrac{W^2}{\rho^2 A}\right]\dfrac{\partial\rho}{\partial h}\Big|_p & A-\left[\dfrac{W^2}{\rho^2 A}\right]\dfrac{\partial\rho}{\partial p}\Big|_h\\ \dfrac{a^2}{\rho A} & \left[\dfrac{Wa^2}{\rho A}\right]\dfrac{\partial\rho}{\partial p}\Big|_h & -\left[\dfrac{Wa^2}{\rho^2 A}\right]\dfrac{\partial\rho}{\partial p}\Big|_h\\ \dfrac{a^2}{A} & -\left[\dfrac{Wa^2}{\rho A}\right]\dfrac{\partial\rho}{\partial h}\Big|_p & \left[\dfrac{Wa^2}{\rho^2 A}\right]\dfrac{\partial\rho}{\partial h}\Big|_p\end{bmatrix}$$

$$\underline{\mathbf{D}}=\begin{bmatrix}-\rho A\left[F+g\dfrac{dH}{dz}\right]+\left[\dfrac{2W^2}{\rho A^2}\right]\dfrac{dA}{dz}\\ a^2\left[Q+\dfrac{WF}{\rho A}\right]\dfrac{\partial\rho}{\partial p}\Big|_h\\ -a^2\left[Q+\dfrac{WF}{\rho A}\right]\dfrac{\partial\rho}{\partial h}\Big|_p\end{bmatrix}=\begin{bmatrix}D_1\\ D_2\\ D_3\end{bmatrix},$$

where the acoustic speed, a, is expressed as follows:

$$a=\left[\frac{\partial\rho}{\partial p}\Big|_h+\frac{1}{\rho}\frac{\partial\rho}{\partial h}\Big|_p\right]^{-1/2}. \tag{7}$$

In the model, constitutive laws are required for the transfer of heat and momentum across system boundaries, and the following relations can be used:

$$Q=\left[\frac{\dot{Q}_w'' P_H}{\rho A}\right]=\left[\frac{h_\infty P_H}{\rho A}\right](T_w-T_\infty) \tag{8}$$

$$F=\left[\frac{\tau_w P_w}{\rho A}\right]=\left[\frac{4f_{lo}}{D_h}\phi_{lo}^2+\frac{K}{L}\right]\frac{W|W|}{2\rho^2 A^2}, \tag{9}$$

where f_{lo} is the friction factor, ϕ_{lo}^2 is the appropriate two-phase multiplier and K/L is the distributed loss coefficient. The choice of appropriate empirical equations for h_∞, ϕ_{lo}^2 and K/L is dependent on the particular problem under consideration. The equation of state, $\rho=\rho(p,h)$, is used. Note also that all the thermodynamic properties of our model are subjected to changes as the pressure drops along the axial direction of the channels. The eigenvalues of matrix $\underline{\underline{\mathbf{A}}}$ determine the mathematical class of Eq. (10); furthermore, all eigenvalues of $\underline{\underline{\mathbf{A}}}$ are real (u, $u+a$, $u-a$) and can therefore be classified as hyperbolic equations. We then use substantial derivatives (namely $\frac{d}{dt}\equiv\frac{\partial}{\partial t}+\underline{V}\cdot\nabla$) to obtain the

compatibility equations by transforming the PDEs into ordinary differential equations along the corresponding characteristics. These equations can be used in a Lagrangian reference frame where spatial and temporal discretizations are not predefined. The characteristic equations and the corresponding compatibility equations are solved simultaneously so that we can obtain all the field variables that define the flow as well as the spatial and temporal grid structures. This method, known as MECA, is accepted as a benchmark solution because it closely follows the physics of the problem and consequently produces accurate results.

In spite of its accuracy, MECA requires considerable computation time and cannot be easily applied to geometrically complex problems. Hence, we used a finite-difference solution that is more flexible, computationally faster and reasonably accurate. The compatibility equations, which are applicable to a Eulerian frame of reference, were also considered and used for further analysis. These compatibility equations can be written in a compact form as follows:

$$\underline{\underline{\mathbf{B}}}\ \frac{\partial}{\partial t}[\underline{\mathbf{U}}]+\underline{\underline{\Lambda}}\ \underline{\underline{\mathbf{B}}}\ \frac{\partial}{\partial z}[\underline{\mathbf{U}}]=[\underline{\mathbf{C}}], \tag{10}$$

where the columns of $\underline{\underline{\mathbf{B}}}^{-1}$ are the eigenvectors of $\underline{\mathbf{A}}$, $\underline{\underline{\Lambda}}$ is a diagonal matrix of the eigenvalues of $\underline{\mathbf{A}}$, and $\underline{\mathbf{C}}=\underline{\underline{\mathbf{B}}}\underline{\mathbf{D}}$. For the EVET model, $\underline{\underline{\mathbf{B}}}$, $\underline{\underline{\Lambda}}$ and $\underline{\mathbf{C}}$ are as follows:

$$\underline{\underline{\mathbf{B}}}=\begin{bmatrix} 1 & -\frac{W}{\rho}\frac{\partial\rho}{\partial h}\big|_p & \left[\frac{A}{a}-\frac{W}{\rho}\frac{\partial\rho}{\partial h}\big|_p\right] \\ 0 & 1 & -\frac{1}{\rho} \\ 1 & -\frac{W}{\rho}\frac{\partial\rho}{\partial p}\big|_h & -\left[\frac{A}{a}+\frac{W}{\rho}\frac{\partial\rho}{\partial p}\big|_h\right] \end{bmatrix}$$

$$\underline{\underline{\Lambda}}=\begin{bmatrix} \frac{W}{\rho A}+a & & \\ & \frac{W}{\rho A} & \\ & & \frac{W}{\rho A}-a \end{bmatrix}\equiv\begin{bmatrix} u+a & & \\ & u & \\ & & u-a \end{bmatrix}$$

$$\underline{\mathbf{C}}=\begin{bmatrix} \rho D_1-\frac{W}{\rho}\frac{\partial\rho}{\partial h}\big|_p\, D_2+\left[\frac{A}{a}-\frac{W}{\rho}\frac{\partial\rho}{\partial p}\big|_h\right]D_3 \\ -\frac{D_3}{\rho}+D_2 \\ \rho D_1-\frac{W}{\rho}\frac{\partial\rho}{\partial h}\big|_p\, D_2-\left[\frac{A}{a}+\frac{W}{\rho}\frac{\partial\rho}{\partial p}\big|_h\right]D_3 \end{bmatrix}=\begin{bmatrix} C_1 \\ C_2 \\ C_3 \end{bmatrix}.$$

Eq. (10) can be approximated by following the left and right difference equations as follows:

$$\underline{\underline{\mathbf{B}}}_k^{\,n}\frac{\underline{\mathbf{U}}_k^{\,n+1}-\underline{\mathbf{U}}_k^{\,n}}{\Delta t}+\underline{\underline{\Lambda}}_k^{\,n}\ \underline{\underline{\mathbf{B}}}_k^{\,n}\frac{\underline{\mathbf{U}}_k^{\,n+1}-\underline{\mathbf{U}}_{k-1}^{\,n+1}}{\Delta z_{k-1}}=\underline{\mathbf{C}}_k^{\,n} \tag{11}$$

$$\underline{\underline{\mathbf{B}}}_k^{\,n}\frac{\underline{\mathbf{U}}_k^{\,n+1}-\underline{\mathbf{U}}_k^{\,n}}{\Delta t}+\underline{\underline{\Lambda}}_k^{\,n}\ \underline{\underline{\mathbf{B}}}_k^{\,n}\frac{\underline{\mathbf{U}}_{k+1}^{\,n+1}-\underline{\mathbf{U}}_k^{\,n+1}}{\Delta z_k}=\underline{\mathbf{C}}_k^{\,n}. \tag{12}$$

Whether the difference form in Eq. (11) or (12) is used depends on the flow character at the mesh point, k. Spatial derivatives are approximated by the left-hand differences when the characteristic is positive and by the right-hand differences when the characteristic is negative. All three equations use a first-order upwind scheme for convective term discretizations, and the upstream point is chosen in relation to the sign of the characteristics. Thus, for the present case of a subsonic flow ($u<a$), the spatial derivatives for the characteristic equations C^+ (i.e., $\Lambda_{11}=u+a$) and C^o (i.e., $\Lambda_{22}=u$) are approximated by the left difference equations, whereas the C^- (i.e., $\Lambda_{33}=u-a$) characteristic equations are approximated by the right difference equations. This choice of finite differencing is necessary as it facilitates a natural way of treating the boundary conditions, such as the velocity and enthalpy or the pressure and enthalpy at the channel inlet for the subsonic flow and the pressure (or the enthalpy or velocity) at the channel outlet.

Let us define matrix $\underline{\underline{\Gamma}}$ such that its diagonal elements are equal to if the slope of the characteristics is positive and 0 if the slope of the corresponding characteristic is negative. Thus, in our subsonic flow,

$$\underline{\underline{\Gamma}}=\begin{bmatrix} 1 & & \\ & 1 & \\ & & 0 \end{bmatrix}.$$

By premultiplying Eq. (11) with $\underline{\underline{\Gamma}}$ and Eq. (12) with ($\underline{\underline{\mathbf{I}}}$ - $\underline{\underline{\Gamma}}$) and then adding the two equations, we get the difference equation for the k^{th} mesh point as follows:

$$\underline{\underline{\mathbf{M}}}_{k,k-1}^{\,n}\ \underline{\mathbf{U}}_{k-1}^{\,n+1}+\underline{\underline{\mathbf{M}}}_{k,k}^{\,n}\ \underline{\mathbf{U}}_k^{\,n+1}+\underline{\underline{\mathbf{M}}}_{k,k+1}^{\,n}\ \underline{\mathbf{U}}_{k+1}^{\,n+1}=\underline{\mathbf{N}}_k^{\,n} \tag{13}$$

where $k=k_{min}+2,k_{min}+3,\ldots,k_{max}-2$.

The 3×3 matrices $\underline{\underline{\mathbf{M}}}_{k,k-1}$, $\underline{\underline{\mathbf{M}}}_{k,k}$ and $\underline{\underline{\mathbf{M}}}_{k,k-1}$ are given by

$$\underline{\underline{\mathbf{M}}}_{k,k-1}=-\underline{\underline{\Gamma}}\ \underline{\underline{\Lambda}}_k\ \underline{\underline{\mathbf{B}}}_k \tag{14}$$

$$\underline{\underline{\mathbf{M}}}_{k,k}=\left[\left(\underline{\underline{\mathbf{I}}}-\underline{\underline{\Gamma}}\right)\lambda_k+\underline{\underline{\Gamma}}\ \lambda_{k-1}-\left(\underline{\underline{\mathbf{I}}}-2\underline{\underline{\Gamma}}\right)\underline{\underline{\Lambda}}_k\right]\underline{\underline{\mathbf{B}}}_k \tag{15}$$

$$\underline{\underline{\mathbf{M}}}_{k,k+1}=\left(\underline{\underline{\mathbf{I}}}-\underline{\underline{\Gamma}}\right)\underline{\underline{\Lambda}}_k\ \underline{\underline{\mathbf{B}}}_k \tag{16}$$

and the column vector $\underline{\mathbf{N}}_k$:

$$\underline{\mathbf{N}}_k=\left[\left\{\left(\underline{\underline{\mathbf{I}}}-\underline{\underline{\Gamma}}\right)\Delta z_k+\underline{\underline{\Gamma}}\ \Delta z_{k-1}\right\}\underline{\underline{\mathbf{D}}}_k+\left\{\left(\underline{\underline{\mathbf{I}}}-\underline{\underline{\Gamma}}\right)\lambda_k+\underline{\underline{\Gamma}}\ \lambda_{k-1}\right\}\underline{\underline{\mathbf{B}}}_k\ \underline{\mathbf{U}}_k^{\,n}\right] \tag{17}$$

where $\lambda_k = \Delta z_k / \Delta t$.

The boiling channel was modeled by dividing into K nodes, where the first node, k_{min}=0, and the last node, k_{max}=K, comprise the boundaries in the axial direction. For k=2 to k=k-2 mesh points, Eq. (13) is used without any changes. For the mesh point k=1, matrix $\underline{\underline{\mathbf{M}}}_{1,0}$ and source vector $\underline{\mathbf{N}}_1$ were adjusted so that the appropriate boundary conditions could be taken care of in accordance with the problems. Similarly, matrix $\underline{\underline{\mathbf{M}}}_{K-1,K}$ and source vector $\underline{\mathbf{N}}_{K-1}$ were modified for K-1 mesh point. To complete the adjustments for the boundary conditions, we used the compatibility equation that corresponds to the C^- characteristics with the help of Eq. (12) for the k=0 mesh point. The compatibility equations that correspond to C^+ and C^o characteristics were then used with the help of Eq. (11) for the k=K mesh point. Thus, the scheme ensures that the boundary conditions are the same as the original problem. Note that when the boundary conditions are applied to the case of our subsonic flow, we need three boundary conditions, two at the inlet and one at the outlet. Finally, an appropriate matrix inversion technique was used to solve the $3 \times K$ simultaneous equations for the same number of unknown variables.

2.2 Steady State Solution

To get the steady state equations, we used Eqs. (1), (2) and (3) and dropped all the terms containing $\frac{\partial}{\partial t}$. The discretized equations used for the steady state solution are as follows:

$$\rho_{i+1} A_{i+1} u_{i+1} = \rho_i A_i u_i \tag{18}$$

$$p_i - p_{i+1} = \frac{1}{2}\left(\frac{1}{A_i} + \frac{1}{A_{i+1}}\right)\left[\left(\rho A u^2\right)_{i+1} - \left(\rho A u^2\right)_i\right] + \frac{1}{2}\left[\left\{\rho\left(F+g\right)\right\}_i + \left\{\rho\left(F+g\right)\right\}_{i+1}\right]\left(z_{i+1} - z_i\right) \tag{19}$$

$$(e_f)_{i+1} - (e_f)_i = \frac{1}{2}\left[\left(\frac{\dot{Q}_w'}{\rho A u}\right)_i + \left(\frac{\dot{Q}_w'}{\rho A u}\right)_{i+1}\right]\left(z_{i+1} - z_i\right). \tag{20}$$

2.2.1 Algorithm to Solve Steady State Equations

The following procedure was used to solve the steady state equations:

1. All properties are known for the i^{th} mesh point of the boiling channel.
2. The density is initially assumed for the next mesh point of i=i+1 and the velocity, u_{i+1}, pressure, p_{i+1}, and enthalpy, h_{i+1}, are calculated with Eqs. (18), (19) and (20) respectively.
3. The density, ρ_{i+1}, is then updated with a thermodynamic equation of state, ρ_{i+1}=ρ_{i+1}(p_{i+1},h_{i+1}).
4. Next, the iteration is continued until the convergence for the density, ρ_{i+1}, is achieved.
5. The same methodology is followed for the next mesh point until the channel outlet is reached.

For FC BWRs, the inlet velocity, pressure and enthalpy are known at a time of t = 0 and the steady state equations are then solved as a means of determining all the properties throughout the channel. The steady state results are used as initial conditions for transient analysis. We used the steady state inlet and outlet pressures as boundary conditions to analyze the in-phase mode of oscillation (or core-wide instability) of the parallel channels of the boiling reactor core. For the NC BWRs, we determined the inlet velocity by using a shooting method to obtain the desired pressure drop across the channels. If a large diameter downcomer is used in NC BWRs, the fixed pressure drop boundary condition can be calculated with the hydrostatic pressure head difference.

2.3 Validation of the Model

Our model developed was validated against a numerical benchmark problem (MECA) described in [1] and the experimental results of Solberg [15].

2.3.1 Comparison with the MECA Results

The specifications of the problem used in MECA are given in Fig. 1, and the initial conditions and boundary conditions are listed in Table 1. For this problem, the

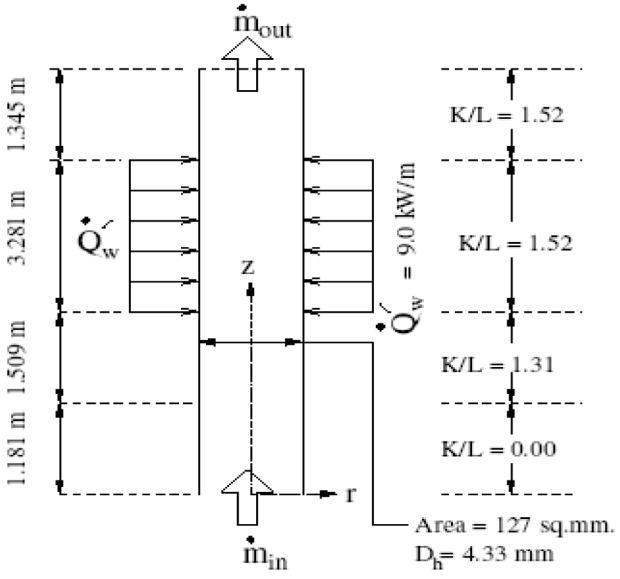

Fig. 1. Specifications of a Vertical Channel of MECA

Table 1. Operating Conditions of a Benchmark Problem

Initial conditions	$u(z)$=1.089 m/s $h(z)$=1184.7 kJ/kg for $o<z<L$
	$p(z)=p(0)-(z/L)[p(0)-p(L)]$
	$p(0)$=7.102 MPa,
	$p(L)$=6.984 MPa
Boundary conditions	$p(0,t)$=7.102 MPa
	$h(0,t)$=1184.7 kJ/kg
	$p(L,t)$=6.984 MPa
	Uniform heat flux of 9000 W/m applied instantaneously starts the transients.

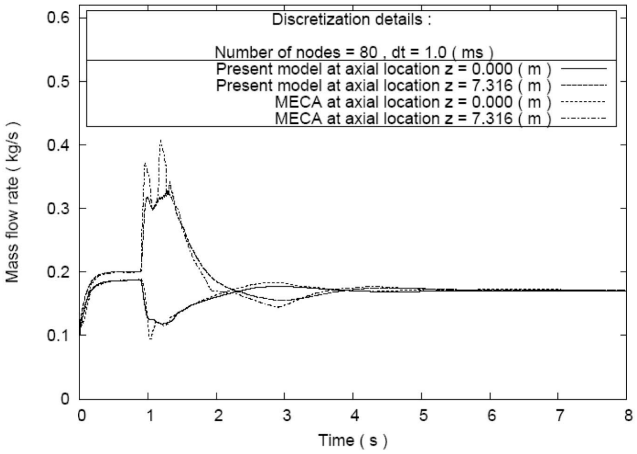

Fig. 2. Variation of the Mass Flow Rate with Time

friction factor, f_{lo}, is given as

$$f_{lo}=\begin{cases}\dfrac{16}{Re} & ;\mathrm{Re}\le 1502\\ 0.046Re^{-0.2} & ;\mathrm{Re}>1502\end{cases}. \tag{21}$$

The following two-phase friction factor developed by Hancox and Nicoll [14] was used:

$$\phi_{lo}^2=\begin{cases}1 & ;x\le 0, x\ge 1\\ 1+x(\beta-1)\left[1+3.57exp(-0.0084\gamma)\right.\\ \left.\times\left\{1-exp\left[-4.96(1-x)\right]\right\}\right] & ;0<x<1\end{cases} \tag{22}$$

where

$$\gamma=\frac{\rho|u|}{\left[g\rho_f(\rho_f-\rho_g)\mu_f\right]^{1/3}};\quad \beta=\frac{\rho_f}{\rho_g}\left(\frac{\mu_g}{\mu_f}\right)^{0.2}.$$

The variations of the mass flow rate and enthalpy with time are shown in Figs. 2 and 3. These results have a very close proximity[1] with the results obtained by MECA [1].

2.3.2 Comparison with Solberg's Experiment

Solberg's experimental test facility consists of a vertical heated section with orifices at the inlet and outlet boundaries. Details of the test section [15] are listed in Table 2. The simulation was conducted to find out the operational regime across which the boiling channels are subjected to instabilities. In the numerical study, the steady state solution was first obtained with the inlet velocity and pressure as shown in Table 2, for the particular

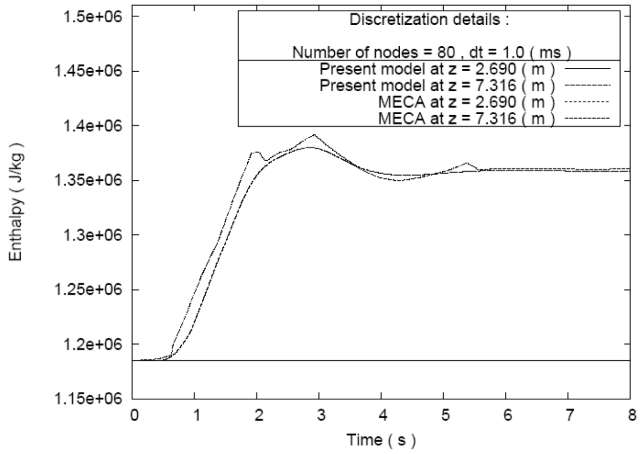

Fig. 3. Variation of Enthalpy with Time

inlet enthalpy and heat flux as obtained through dimensionless numbers, N_{sub} and N_{pch}. Next, the model uses these results as initial conditions for the transients generated by perturbations of steady state inputs. Depending on the converging or diverging amplitude of the oscillations, the system response confirms whether the boiling channel is in a stable or unstable zone. As shown in Fig. 4, an MSB was obtained in non-dimensional parameter space (i.e., a phase change-subcooling plane) and then used to compare our results with the experimental data points. The comparison confirms close agreement between the two sets of results.

2.4 Effect of Various Parameters on Stability

Various parametric studies have evaluated the performance of water cooled reactors under FC and NC

[1]It is obtained when $f_{lo}\times\phi_{lo}^2$ is taken as recommended by Ferch [3].

Table 2. Specifications of a Vertical Test Section of Solberg's Experiment

Geometrical parameters		Operating conditions	
Diameter	5.25 mm	Inlet	80
Length	2.90 m	pressure	atm (BC)
K_i	35.60	Inlet	47800
K_e	0.06	Reynolds no.	(IC)
Working fluid : water		$f_{2\phi} = 2 \times f_{1\phi}$	

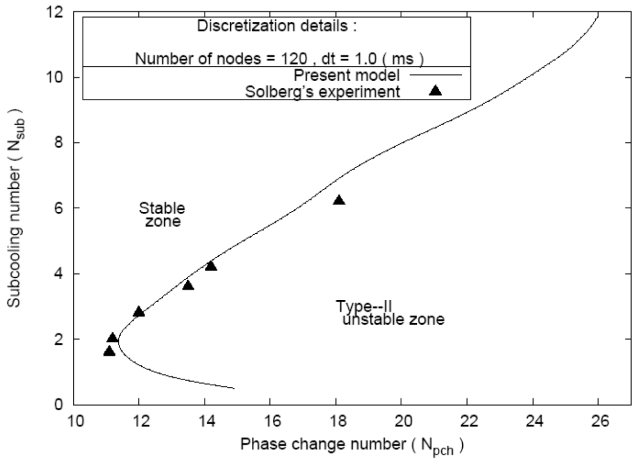

Fig. 4. Comparison with Solberg's Experiments

Table 3. Specifications of a BWR/6

Operating conditions	
Working coolant	Water
Rated power	3950 MW
Rated flow	13100 kg/s
Inlet pressure	7.17 MPa
Inlet temperature	551.15 K
Fuel assembly data	
Active fuel length	3.81 m
Number of fuel bundles	748
Number of fuel rods	62
Rod array (square)	8×8
Rod pitch	16.2 mm
Fuel rod data	
Pellet diameter	10.4 mm
Clad outside diameter	12.27 mm
Clad thickness	0.813 mm
Friction factor used	
$f_{2\phi} = \phi_{lo}^2 \times f_{1\phi}$	$\phi_{lo}^2 = 2.0$
$f_{1\phi} = 16/Re$	for laminar flow
$f_{1\phi} = 0.046 Re^{-0.20}$	for turbulent flow

modes of heat transfer cooling systems. The BWR/6 is representative of FC channels and its relevant data [16] are listed in Table 3. Table 4 provides the information (taken from Lin et al. [8]) on NC water cooling channels. In the case of forced flow systems, the mass flow rate is independent of channel dynamics; furthermore, neither the heat flux nor inlet subcooling can affect the mass flow rate. In the case of NC systems, loop dynamics plays an important role in deciding the mass flow rate in the channels; in addition, the heat flux shape, the inlet subcooling, and the channel geometries influence the loop mass flow rate, which in turn affects the stability of the boiling channels. An increase in the mass flow rate has a stabilizing effect on the boiling channels because it reduces the void fraction (or quality) of the two-phase mixture in the channels; thus, the total two-phase frictional pressure drop decreases. Note also that the two-phase frictional pressure drop is the more delayed component as compared to the single-phase frictional pressure drop and therefore very influential in triggering DWOs in the boiling channels.

To evaluate the performance of different BWRs at various operating conditions, we chose a dimensionless parameter space, where the subcooling number (N_{sub}) corresponds to the inlet subcooling rate and the phase change number (N_{pch}) represents the total power with respect to the unit characteristic mass flow rate. Because the mass flow rate is independent of channel geometry, the inlet subcooling, and the power levels of FC BWRs, the steady state mass flow rate can be taken as the characteristic mass flow rate. The loop mass flow rate for NC BWRs varies in relation to the channel dynamics. Accordingly, we used a predefined characteristic mass flow rate (that can be set as intended) as a fixed reference while comparing our results under different operating conditions.

Figures 5 to 7 provide insight into various nonlinear oscillatory phenomena of BWR/6 at three equilibrium

Table 4. Specifications of an NC Loop

Geometrical parameters		Operating conditions	
L_H	2.44 m	Inlet	68.947 bar
D_H	13.20 mm	pressure	(BC)
k_{hr}	2(1-S)S	Pressure	$\rho_f gL$
k_e	0.00	drop	(BC)
Working fluid : water		$f_{2\phi} = 2 \times f_{1\phi}$	
$f_{1\phi}$=0.213/$Re^{0.241}$		$u_s = \frac{1.62 g^{0.569} D_H^{0.705}}{\nu^{0.137}}$	

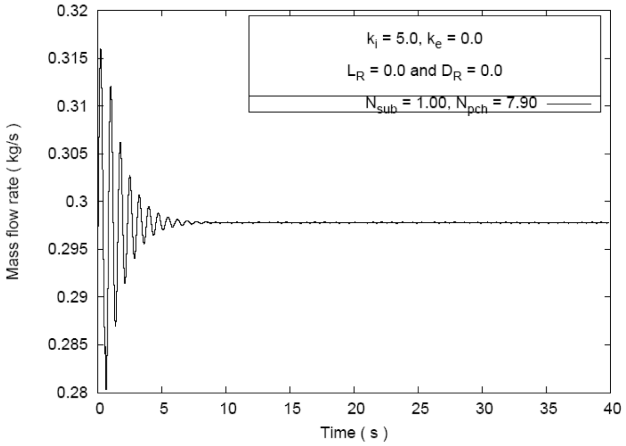

Fig. 5a. Variation of the Inlet Mass Flow Rate with Time at a Stable Pont (BWR/6)

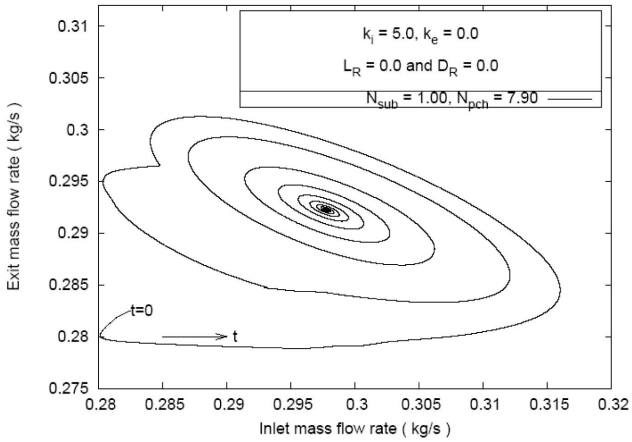

Fig. 5b. Time Evolution of the Inlet and Outlet Mass Flow Rates in a Phase Plane Diagram at a Stable Pont (BWR/6)

points close to the MSB. The time evolution of the inlet mass flow rate, after an initial perturbation at a stable equilibrium point, is shown in Fig. 5a. The phase plane diagram (Fig. 5b) of the inlet and exit mass flow rates confirms the existence of a stable point where the flows converege to a single point attractor. The simulations of Figs. 6a and 6b show the limit cycle oscillations at the MSB. These figures are aimed at showing how a thermal-hydraulics solver can simulate the limit cycle oscillations. The oscillatory behavior of the reactor around an unstable point is represented in Figs. 7a and 7b. Following the initial perturbation, the oscillation amplitude of the flow variables at an unstable condition grows initially but essentially approaches the limit cycle oscillations after a considerable time has elapsed.

2.4.1 Effect of a Riser on Different BWRs

The introduction of adiabatic riser sections affects the performance of different reactors in various ways as follows:

1. A riser acts as a destabilizing agent for FC BWRs. It shifts MSBs to the left (Fig. 8), indicating that the boiling channels are being destabilized at lower power due to the increase of the two-phase frictional pressure drop that takes place in the upper half of the channels; there is also an increase in the time-delayed pressure drops. Moreover, Fig. 8 confirms that there is no type-I instability associated with FC BWRs.
2. In the case of NC BWRs, risers have opposite effects under different operating conditions. Type-I and type-II instabilities are both possible whenever a riser is installed.
3. The introduction of a riser in NC loops increases the two-phase friction length and the gravity pressure head. The former has a destabilizing effect whereas the latter causes a higher mass flow rate, which in turn acts as a stabilizing agent. Note also that the effect of the latter is more dominant because a longer riser section enhances the circulation flow rate, thereby reduing the maximum channel void fraction and the two-phase frictional pressure drop. Figure 9 confirms that the type-

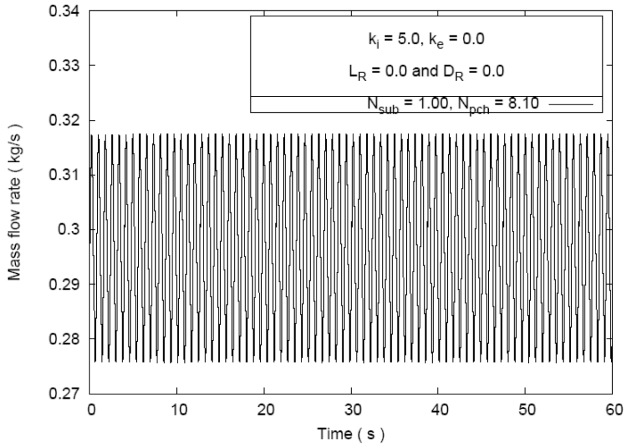

Fig. 6a. Variation of the Inlet Mass Flow Rate with Time at a Limit Cycle Oscillation (BWR/6)

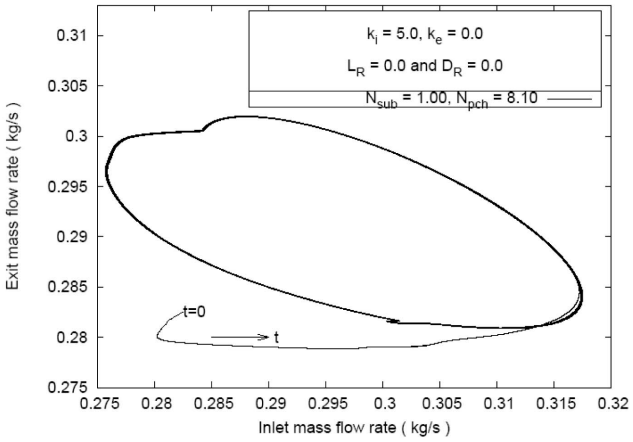

Fig. 6b. Time Evolution of the Inlet and Outlet Mass Flow Rates in a Phase Plane Diagram at a Limit Cycle Oscillation (BWR/6)

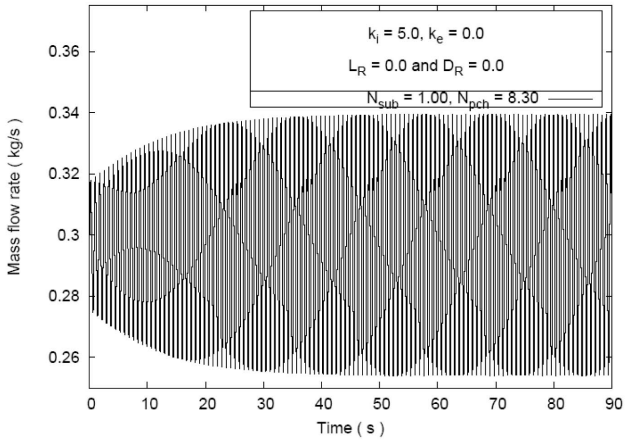

Fig. 7a. Variation of the Inlet Mass Flow Rate with Time at an Unstable Point (BWR/6)

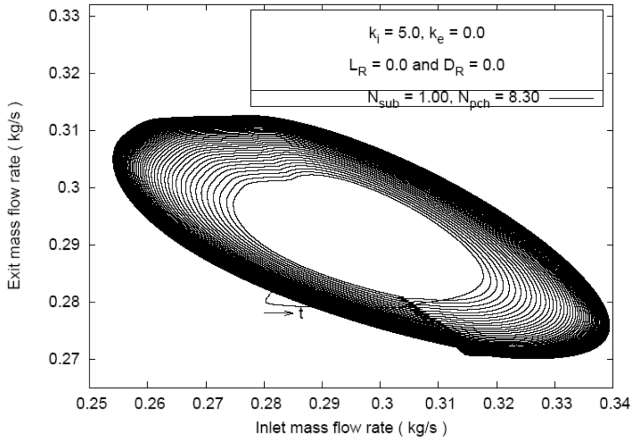

Fig. 7b. Time Evolution of the Inlet and Outlet Mass Flow Rates in a Phase Plane Diagram at an Unstable Pont (BWR/6)

II stability shifts to the right at higher power levels for the same inlet subcooling.

4. Figure 9 also shows that the type-I unstable zone increases when the riser length increases for NC BWRs. This increase occurs because of a reduction in the maximum void fraction in the channel, though the lower two-phase frictional pressure drop causes a large gravitational pressure drop. In the gravity dominated region, the gravitational pressure drop becomes more influential than the frictional pressure drop; thus, type-I instability, which originats from the gravitational pressure drop, occurs whenever the riser length increases.
5. Figure 10 shows that an option of a riser with a relatively small diameter is not very efficient at enhancing the circulating flow speed of the channel because such a riser increases the frictional pressure drop.

2.4.2 Effect of the Axial Heat Profile on Different BWRs

In this section we present our analysis of how variations in the axial heat flux affect the stability of different boiling channels. The model, which is simulated with a symmetric sinusoidal axial heat profile, was compared with the results obtained for a uniform heat flux profile. The comparative observations are described as follows:

1. For FC BWRs, as shown in Fig. 11, a sinusoidal axial heat profile enlarges the stability region. For both uniform and sinusoidal flux profiles, the boiling boundary takes place in the bottom half of the channel but for the uniform heat flux profile, the boiling boundary occurs relatively earlier than the sinsoidal flux profile, causing larger two-phase friction length. However, because the total power is the same, the

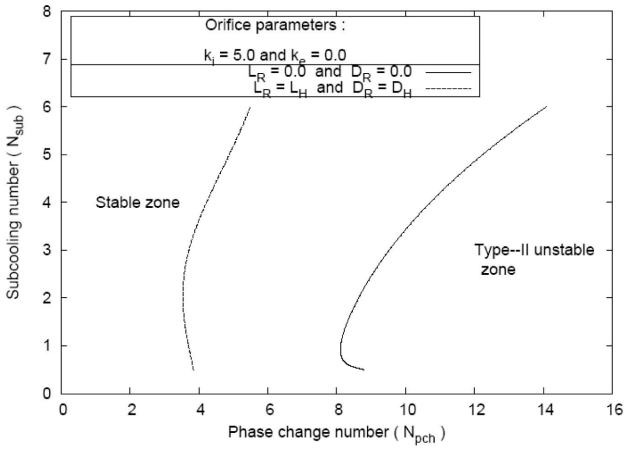

Fig. 8. Effect of a Riser On an FC BWR/6

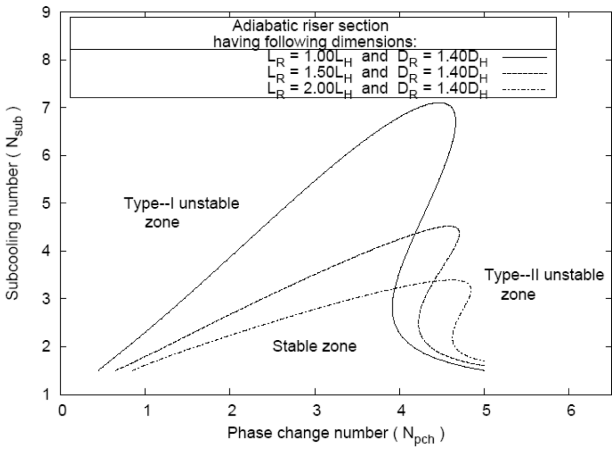

Fig. 9. Effect of the Riser Length On an NC Loop

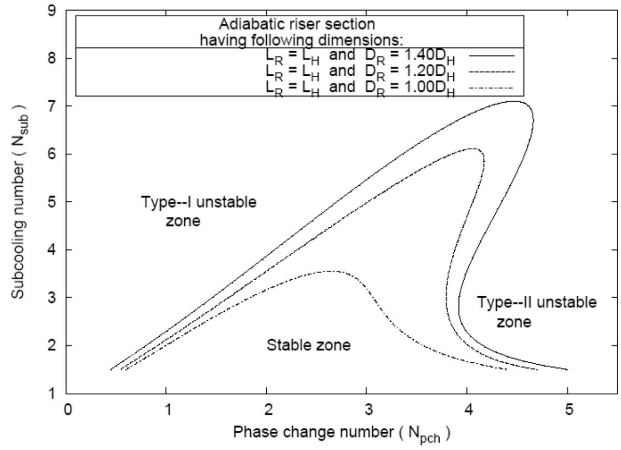

Fig. 10. Effect of the Riser Diameter on an NC Loop

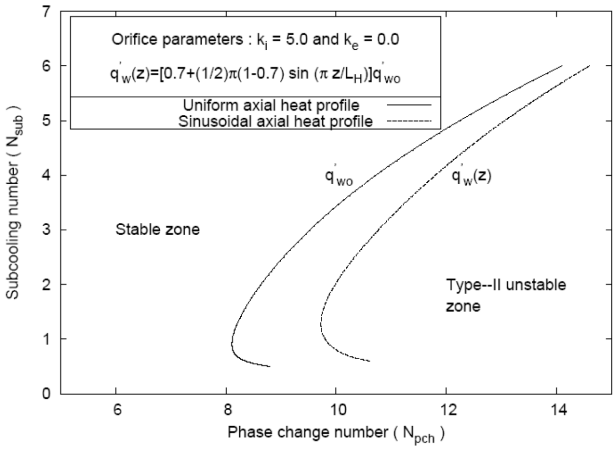

Fig. 11. Effect of a Sinusoidal Axial Heat Profile On an FC BWR/6

conservation of energy implies that exit quality of the two-phase mixture decreases. This phemenon leads to two opposing effects on the total frictional pressure drop. Because the lowering of boiling boundary is dominant, a uniform axial heat profile is more destabilizing than the sinusoidal profile. Note also that the difference in the unstable zone due to these two different heat profiles becomes narrower at a high subcooling number because the increase in the two-phase friction length with a uniform axial heat profile becomes less significant.

2. In the case of NC BWRs, a uniform axial heat profile shifts the boiling boundary downwards, thereby increasing the two-phase friction length. Thus, the same effect is observed for both NC and FC BWRs with regard to type-II instability (Fig. 12) in the friction-dominated region. However, for high inlet subcooling, the difference in unstable regions does not become narrower for NC BWRs (as it does for FC BWRs). It is observed that at high subcooling number, sinusoidal heat flux shape causes the boiling boundary to shift more downwards and accordingly, it should have been more unstable than the other one (which is not the case in Fig. 12). On the contrary, it is also observed that the circulation mass flow rate increases in case of sinusoidal axial heat flux profile and as a result, the system becomes more stable.
3. In the case of NC BWRs, whenever there is a gravity-dominated region at low power levels and a small mass flow rate, the type-I instability region tends to be reduced for the bottom peaked power profiles. Thus, a uniform heat flux profile has a greater stability margin than the other type of profile. The greater stability margin is due to the fact that the bottom peaked power profile increases the two-phase friction length and reduces the maximum void fraction of the channel because the total power is the same and, as a result, there is a higher gravitational pressure drop, which dominates at the particular operating conditions. Consequently, the loop mass flow rate increases and the system becomes more stable to compensate for the total pressure drop, which is fixed.

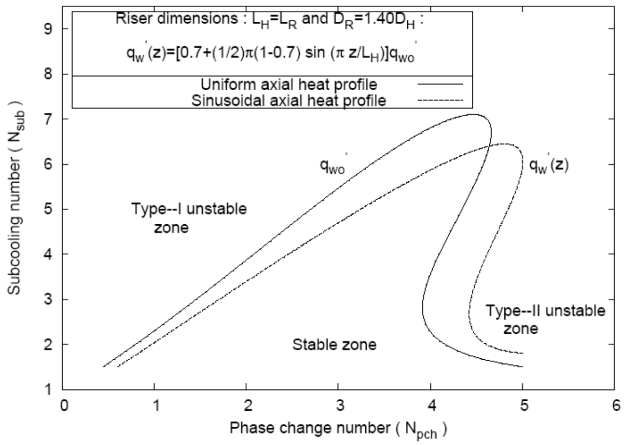

Fig. 12. Effect of a Sinusoidal Axial Heat Profile On an NC Loop

3. CONCLUSION

A mathematical model was developed to simulate the hydrodynamics of flow boiling systems. The nonlinear conservation equations are systematically transformed into a characteristic form and an implicit characteristics-based finite-difference scheme is used to solve the equations numerically in a Eulerian reference frame. A steady state algorithm is then developed and both the steady state model and the transient model are used to analyze the DWOs. The model is accurate, computationally efficient, and flexible; it also treats the boundary conditions naturally, takes into account the compressibility effect of the two-phase flow, and can be implemented in an easy and versatile manner to analyze various accidental situations with a few approximations. The model, which was validated with available numerical and experimental benchmarks, is robust enough to handle spatially varying time-dependent heat sources. This capabililty is essential for a scheme that incorporates a space-time kinetic neutronics model coupled with a thermal hydraulics code for simulating commercial BWRs under realistic conditions.

We analyzed the effect of adiabatic riser sections on type-I and type-II instabilities under different operating conditions and investigated how the stability dynamics differs for FC and NC boiling channels. FC BWRs are subjected to only type-II instabilities, whereas both type-I and type-II instabilities can occur when risers are introduced to NC BWRs. Risers cannot be installed in FC BWRs because they significantly increase the unstable zone. However, risers of proper geometrical dimensions for NC BWRs are very important because they can enhance the stability margin in terms of type-II instability. On the other hand, risers have an adverse effect because they lengthen the type-I instability zone whenever there is low power and a small mass flow rate, as in the case of start-up conditions. Although we set the two-phase multiplier value at $\phi_{lo}^2 = 2.0$, the conclusions with regard to the stabilizing or destabilizing effect of the riser for various types of BWRs remain valid for different values of ϕ_{lo}^2. The axial variation of the heat flux shape is also important in determining the stability margins of BWRs. The bottom peaked power profile generally shortens the stability boundary for all reactors under normal operating conditions (namely, for high power levels and friction dominated regions) but has a positive effect by increasing the stability region of NC BWRs in gravity-dominated regions.

4. SCOPE OF FUTURE WORK

Our model has been tested extensively under various operating conditions. In addition, the numerous parametric studies on the model are being used to analyze the flow-induced in-phase modes of oscillations for FC and NC water channels. The model can be extended to analyze parallel channel instability during an out-of-phase mode of oscillations. The essence of the method of simulating the out-of-phase mode of oscillations lies in imposing the right boundary conditions in a proper sequence. We are now in the process of integrating the thermal hydraulics code with a 3-D, transient neutronics model that can analyze the void-reactivity and Doppler feedback effects during DWOs for water cooled boiling reactors.

ACKNOWLEDGEMENTS

This work was done as part of the PhD project of the first-named author. The authors gratefully acknowledge the help received from Indian Institute of Technology, Bombay, in providing access to the computational facilities of the Mechanical Engineering Department. They also thank the All India Council of Technical Education for the scholarship support of the first-named author. Finally, they express deep gratitude to Mr. Supreet Singh Bahga, a senior undergraduate student, for his assistance in the development of the computational model.

NOMENCLATURE

A	Cross-sectional area	(m^2)
a	Acoustic speed	(m/s)
D	Diameter	(m)
D_h	Hydraulic diameter	(m)
e	Total specific internal energy	(J/kg)
e_f	Total specific flow energy	(J/kg)
f	Friction factor	(dimensionless)
f_{lo}	Friction factor for single phase liquid	(dimensionless)
G	Mass velocity	(kg/m^2 s)
g	Acceleration due to gravity	(m/s^2)
H	Vertical height	(m)
h	Specific enthalpy	(J/kg)
h_∞	Heat transfer coefficient	(W/m^2 K)

k Orifice coefficient $\left[\frac{1}{2}\frac{\Delta p}{\rho u^2}\right]$ (dimensionless)
L Length; $L=L_H+L_R$ (m)
$\dot{m}$ Mass flow rate (kg/s)
N_{pch} Phase change number $\left[\frac{\dot{Q} v_{fg}}{A u_s h_{fg}}\right]$ (dimensionless)
N_{sub} Subcooling number $\left[\frac{(h_f - h_{in}) v_{fg}}{h_{fg} v_f}\right]$ (dimensionless)
n_r Channel number under consideration (dimensionless)
P_H Heated perimeter (m)
P_w Wetted perimeter (m)
p Pressure (Pa)
$\dot{Q}$ Total heat power (W)
$\dot{Q}'$ Linear heat rate (W/m)
$\dot{Q}''$ Heat flux (W/m)
Re Reynolds number (dimensionless)
r Radial axis (m)
S Heater and riser area ratio; $S=\left[\frac{A_H}{A_R}\right]$ (dimensionless)
T Temperature (K)
T_∞ Coolant temperature (K)
t Time (s)
u Fluid velocity in axial direction (m/s)
u_s Characteristic fluid velocity (m/s)
$\underline{V}$ Velocity vector (m/s)
W Mass flow rate (kg/s)
x Vapor quality (dimensionless)
z Axis in axial direction (m)

Greek Symbols

α Void fraction (dimensionless)
θ Azimuthal angle (degree or radian)
μ Dynamic viscosity (kg s/m)
v Kinematic viscosity (m^2/s)
ρ Density (kg/m^3)
τ Shear stress (N/m^2)
ϕ_{lo}^2 Two-phase flow multiplier (dimensionless)
$\underline{\underline{\Phi}}$ Matrix Φ
$\underline{\Phi}$ Vector Φ

Superscripts

n Time step

Subscripts

e Exit
f Saturated liquid
H Heater
hr Junction between heater and riser
i Inlet
in Inlet
g Saturated vapour
k Index used for spacial discretization
out Outlet
R Riser
w Wall
2ϕ Two-phase
1ϕ Single-phase

Abbreviations

BC Boundary condition
IC Initial condition

REFERENCES

[1] W.T. Hancox and S. Banerjee, "Numerical Standard for Flow Boiling Analysis", *Nuclear Science and Engineering*, **64**, pp. 106-123, (1977).
[2] S. Banerjee and W.T. Hancox, "On the development of methods for analyzing transient flow-boiling", *Int. J. Multiphase Flows*, **4**, pp. 437-460, (1978).
[3] R.L. Ferch, "Method of Characteristics Solutions for non-equilibrium transient flow-boiling", *Int. J. Multiphase Flow*, **5**, pp. 265-279, (1979).
[4] D.R. Liles and W.H. Reed, "A semi-implicit method for two-phase fluid dynamics", *Journal of Computational Physics*, **26**, pp. 390-407, (1978).
[5] V. Chatoorgoon, "Sports -- A Simple Non-Linear Thermal Hydraulic Stability Code", *Nuclear Engineering and Design*, **93**, pp. 51-67, (1986).
[6] R. Prasad, J.B. Doshi and K. Iyer, "A Numerical Investigation of Nuclear Coupled Density Wave Oscillations", *Nuclear Engineering and Design*, **154**, pp. 381-396, (1995).
[7] S. Narayanan, B. Srinivas, S. Pushpavanan and S.M. Bhallamudi, "Non-linear dynamics of a two phase flow system in an evaporator: The effects of (i) a time varying pressure drop, (ii) an axially varying heat flux", *Nuclear Engineering and Design*, **178**, pp. 279-294, (1997).
[8] Y.N. Lin and C. Pan, "Non-linear analysis for a natural circulation boiling channel", *Nuclear Engineering and Design*, **152**, pp. 349-360, (1994).
[9] F.S. Wang, L.W. Hu and C. Pan, "Thermal and stability analysis of a two-phase natural circulation loop", *Nuclear science and Engineering*, **117**, pp. 33-46, (1994).
[10] D.D.B.V. Bragt and T.H.J.J.V.D. Hagen, "Stability of natural circulation boiling water reactors: part I--Description stability model and theoretical analysis in terms of dimensionless groups", *Nuclear Technology*, **121**, pp. 40-51, (1998).
[11] D.D.B.V. Bragt and T.H.J.J.V.D. Hagen, "Stability of natural circulation boiling water reactors: part II--Parametric study of coupled neutronic-thermohydraulic stability", *Nuclear Technology*, **121**, pp. 52-62, (1998).
[12] Rizwan-uddin and J.J. Dorning, "Nonlinear Dynamics of two-phase flow in multiple parallel heated channels", *Two-Phase Flow and Heat Transfer*, **197**, p. 63, (1992).
[13] Rizwan-uddin, "Effects of double-humped axial heat flux variation on the stability of two-phase flow in heated channels", *Int. J. Multiphase Flows*, **20**, No. 6, pp. 1129-1142, (1994).
[14] W.T. Hancox and W.B. Nicoll, "A wall shear stress formula for adiabatic two-phase flow", *Westinghouse Canada Limited Report*, unpublished, 1972.
[15] K. Solberg, "Resulats des Essais d'Instabilities sur la Boucle 'Culine' et Comparisons avec Code de Calcul", *C.E.N.G.*, Note 225, Centre d'Etudes Nucleaires de Grenoble, France 1966.
[16] N.E. Todreas and M.S. Kazimi, "Nuclear Systems I : Thermal Hydraulic Fundamentals", *Hemisphere Publishing Corporation, New York, First Edition*, 1989.